Speed of sound and equation of state for fluid oxygen to 10 GPa

E. H. Abramson, L. J. Slutsky, M. D. Harrell, and J. M. Brown

Citation: The Journal of Chemical Physics **110**, 10493 (1999); doi: 10.1063/1.478979
View online: http://dx.doi.org/10.1063/1.478979
View Table of Contents: http://scitation.aip.org/content/aip/journal/jcp/110/21?ver=pdfcov
Published by the AIP Publishing

Speed of sound and equation of state for fluid oxygen to 10 GPa

E. H. Abramson and L. J. Slutsky
Department of Chemistry, University of Washington, Seattle, Washington 98195

M. D. Harrell
Department of Geological Sciences, University of Washington, Seattle, Washington 98195

J. M. Brown
Geophysics Program, University of Washington, Seattle, Washington 98195

(Received 25 January 1999; accepted 9 March 1999)

The speed of sound in supercritical, fluid oxygen has been measured up to the freezing points of 6.0 GPa at 30 °C and 10.5 GPa at 200 °C. The oxygen was contained in a diamond–anvil cell and pressure was measured on the ruby scale. The measurements were used to establish an equation of state. Additionally, the fluid-β phase boundary was determined between 15 and 180 °C to a precision of 0.02 GPa. © *1999 American Institute of Physics.* [S0021-9606(99)50521-7]

INTRODUCTION

The properties of highly compressed matter are of consequence to a broad variety of disciplines. Some of the direct applications are obvious: the modeling of planetary physics, of explosions and of various areas of industrial interest such as high-pressure tribology would all benefit from a more detailed knowledge both of the thermodynamic and of the transport properties of materials under appropriate conditions. Less directly, a knowledge of how molecules interact when forced significantly closer than mean distances normally explored in the laboratory will serve to improve our understanding of diverse ''low pressure'' phenomena such as sputtering and barriers to diffusion and reaction.

Much of our knowledge of compressed matter comes from x-ray studies of the equations of state of crystals, either in the diamond–anvil cell or the multianvil press. These data allow the testing of various calculational techniques and, perhaps consequently, models meant to reproduce the solid equation of state (EOS) have become reasonably successful. Significantly less information is available on highly compressed fluids. Further, there is reason to suppose that the interaction potentials which reproduce the equations of state of highly symmetrical solids may not be as appropriate for a less symmetric fluid environment or, even within solids, the calculation of transport phenomena which involve vibrational distortions of crystalline symmetry. Appropriately detailed data from fluids are therefore desirable. The ideal system for study would be both fairly simple and capable of significant compression.

Molecular oxygen remains a fluid up to the unusually high pressure of 5.8 GPa at 25 °C and 10.5 GPa at 200 °C; at the higher pressures its density is over twice that of the normal, cryogenic liquid. An overview of previous work on the thermodynamics of fluid oxygen is given by Wagner and Schmidt.[1] These authors have generated a fundamental equation[1,2] which, in the region of higher pressures and temperatures, is based on densities measured up to 0.08 GPa and 30 °C,[3,4] and to 0.03 GPa and 130 °C,[5] combined density and heat capacities measured to 0.03 GPa and 30 °C (Ref. 6) and speeds of sound, also to 0.03 GPa and 30 °C.[7] Other recent data, not used by Wagner and Schmidt, are those of Tsiklis and Kulikova,[8] who measured densities to 1 GPa and 400 °C with a stated accuracy of 2%. Additionally, measurements of density and total internal energy have been made in shocked oxygen up to 86 GPa.[9]

Here, we present a study of the velocity of sound in fluid oxygen along two isotherms of 30 and 200 °C. Each isotherm was followed up to its freezing point.

EXPERIMENT

Oxygen (99.999%) was loaded as a cryogenic liquid into a diamond–anvil cell of the Merrill–Basset type with a gasket made of either 301 stainless steel or Inconel 718. Typical samples were contained in a cylindrical volume 300 μm in diameter and 20–50 μm in thickness. Temperatures were measured with chromel–alumel thermocouples. Pressure measurements were based on the ruby fluorescence scale[10] (R_1 line) with the spectra fit as sums of Gaussian and Lorentzian functions as described by Munro *et al.*[11]

Sound velocities were measured through use of impulsive stimulated scattering, which has been previously described.[12] Briefly, two 80 ps pulses from a Nd:YAG laser are directed into the sample at an intersection angle θ. Overlapping both spatially and temporally, they give rise to an interference pattern of wavelength d given by

$$\lambda = 2d \sin(\theta/2),$$

where λ is the laser wavelength, 1064 nm. Absorption of energy by the sample results in the impulsive launching of two counter-propagating acoustic waves with wavelength d. A third, probe pulse from the same laser is subsequently scattered off the sound waves at the Bragg angle. The intensity of the scattered probe beam is temporally modulated by the amplitude of the wave and, observed as a function of delay time, gives the frequency ν, and hence the velocity $c = d\nu$. Typically, speeds of sound were measured to an accuracy of $\pm 0.2\%$ while pressures were measured to a precision of 0.02 GPa at 30 °C and 0.05 GPa at 200 °C.

Rubies, after grinding to tens of microns, appear to have residual strains which are often large enough to offset the

TABLE I. Speeds of sound as measured at various pressures along isotherms of 30 °C and 200 °C, and also along a nominal isobar of 2.5 GPa.

P (GPa)	*T* (°C)	*c* (km s^{-1})
0.18	30	0.985
0.62	30	1.702
0.76	30	1.825
1.29	30	2.248
1.55	30	2.397
1.94	30	2.605
2.84	30	2.974
3.87	30	3.309
5.44	30	3.716
6.27	30	3.874
0.51	200	1.417
0.93	200	1.895
1.21	200	2.097
1.68	200	2.357
2.18	200	2.633
2.76	200	2.892
3.31	200	3.108
4.08	200	3.326
5.61	200	3.737
7.25	200	4.089
7.36	200	4.089
8.97	200	4.358
10.74	200	4.594
2.84	22	2.974
2.44	148	2.792
2.47	250	2.768
2.51	300	2.767

wavelength of their fluorescence by an amount equivalent to a pressure increment of ~0.05 GPa, and occasionally as much as 0.2 GPa. Annealing at 1000–1100 °C for several hours decreases both the magnitude and frequency of these deviations; it is still common to find rubies which differ reproducibly by the equivalent of 0.02 GPa. The most precise work we have done has been on the melting curve, in which the relative wavelengths of rubies were recorded at 0 GPa and the high-pressure results corrected by the same amounts. The reference rubies at 0 GPa were kept in the same temperature controlled housing as were the samples both because wavelength shifts equivalent to 0.01 GPa are generated by temperature differences of 0.5 °C and because of the desirability of matching as closely as possible the two spectral lineshapes. The power of the exciting laser was attenuated sufficiently that it had no discernable effect on the calculated pressures. With hydrostatic samples we are able to measure pressures with a precision of slightly better than 0.01 GPa. The spectra are measured with a combination of CCD camera and monochromator which give a dispersion of 0.12 Å/bin. The precise measurement of pressures at temperatures higher than about 300 °C was not possible due to the broadening of the ruby fluorescence spectrum.

RESULTS

Measured speeds of sound are listed in Table I and plotted against pressure in Fig. 1. In addition to points along the two isotherms, data were taken at several temperatures along an approximation to an isobar. These latter data, corrected by use of the local pressure derivative to a nominal 2.5 GPa, are shown in Fig. 2; the variation of speed with temperature is adequately approximated by a straight line.

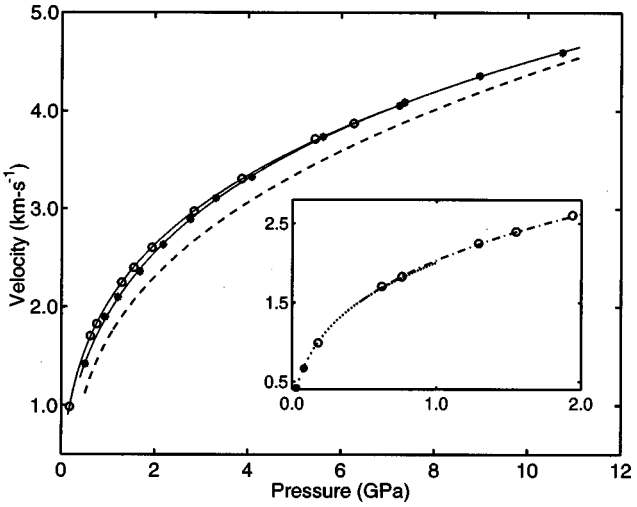

FIG. 1. The measured speed of sound in fluid oxygen is plotted against pressure. Open circles represent data at 30 °C and asterisks data at 200 °C. Solid lines represent fits through the data while the dashed line gives the velocities at 200 °C predicted by Ref. 17. The inset shows an expanded region at low pressures with filled circles representing velocities as predicted by the equation of state of Wagner and Schmidt. The dotted line and dot-dashed line represent the velocities of fluid nitrogen as given, respectively, by Refs. 13 and 15 and scaled as described in the text.

The velocities fair nicely into those of Wagner and Schmidt's model. It seems likely that the measured velocities represent those of the relaxed liquid. A limited search for dispersion was made at 30 °C and 1.5 GPa at frequencies of 1.3, 0.77, and 0.27 GHz. Over this range (limited by the geometry of the diamond–anvil cell) velocities matched to within our uncertainties, i.e., ±0.2% for the two higher frequencies and ±0.5% for the lowest.

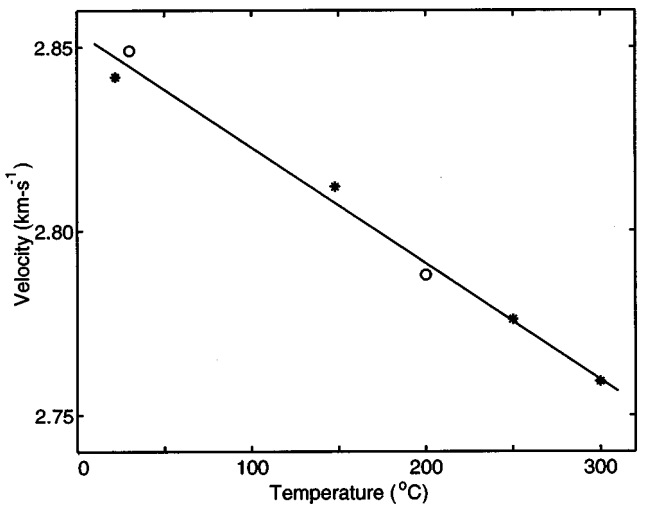

FIG. 2. Speeds of sound are plotted against temperature for a single isobar of 2.5 GPa. The asterisks represent single measurements given in Table I, corrected to 2.5 GPa, while the circles give the values of the 30 °C and 200 °C isotherms (Fig. 1) interpolated to 2.5 GPa. The line is drawn as a visual aid.

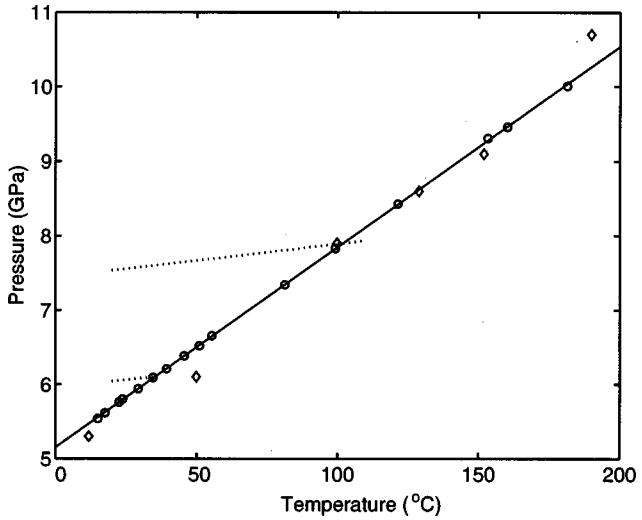

FIG. 3. The melting pressure of oxygen is plotted against temperature. Open circles and the straight, solid line represent our data with a least-squares fit drawn through them. The diamonds represent data from Ref. 20 (which extend past the β-ϵ-fluid triple point at about 370 °C and 16 GPa). Two calculated isochores for the β phase are given by dotted lines.

In the temperature range under consideration fluid oxygen freezes at high pressure to form the crystalline β phase. In an ancillary set of experiments the fluid-β boundary was determined between 15 °C and 180 °C. Each point of equilibrium was established by a visual observation of the simultaneous presence of both phases. The data, shown in Fig. 3, are well represented by the line $P(\mathrm{GPa}) = 0.0270\,T(^\circ\mathrm{C}) + 5.153$ with a root-mean-square misfit of 0.015 GPa. Among observations, the volume of solid varied from approximately 5% to 95% of the sample; no correlation was apparent between the deviations of the data from the fit and the fraction of solid. Since any impurities are likely to have been concentrated in the fluid, this fact suggests strongly that impurities had no significant effect on the melting curve.

ANALYSIS

In principle, once the velocities of sound are measured one can start with known values of density and heat capacity at a low pressure and recursively integrate

$$\left(\frac{\partial \rho}{\partial P}\right)_T = \frac{1}{c^2} + \frac{T\alpha^2}{c_p} \tag{1a}$$

and

$$\frac{\partial c_p}{\partial P} = -T\frac{\partial^2 V}{\partial T^2} \tag{1b}$$

to establish an equation of state. Here ρ, c, α, c_p, and V are, respectively, the mass density, speed of sound, volume coefficient of thermal expansion, specific heat, and specific volume. However, our data, taken in a diamond–anvil cell, do not extend to pressures sufficiently low so as to overlap the range of validity of the Wagner and Schmidt EOS. Further, the variation of speed of sound with temperature is small enough to be obscured, especially at the lower pressures, by uncertainties in the measurement of the pressure. We have established that different methods of interpolating between our data and the potential of Wagner and Schmidt can lead to large differences in the final calculated densities. In order to circumvent this difficulty we estimate the starting densities and heat capacities for our calculations through use of the principle of corresponding states in conjunction with data for nitrogen.

At moderate pressures the EOS of nitrogen and oxygen are very similar when scaled by the critical constants; at 30 °C the reduced densities of oxygen up to 0.08 GPa (the highest pressure for which accurate densities were reported) differ by less than 1% from those of nitrogen when evaluated at the same reduced temperatures and pressures. A comparison of the shocked materials[9] also shows a good correspondence to over 40 GPa and densities over 2.9 g/cm^{-3}, albeit at the much higher temperatures (and uncertainties) associated with the typical Hugoniot curve. Less accurate measurements of density,[8] up to 0.6 GPa at 20 °C and 100 °C, agree with scaled nitrogen to within their random error of roughly 2%.

The scaled velocities of sound may also be calculated through use of Eq. (1a) with ρ, P, T, and α scaled by the critical constants, ρ additionally scaled by the molecular masses, and C_p given by $C_p = 7R/2 + C_{p\,\mathrm{excess}}$, where $C_{p\,\mathrm{excess}}$ is to be scaled by the appropriate ratios of critical constants. In the range where the Wagner and Schmidt EOS may be considered accurate, the velocities of oxygen are within 1% of the equivalent velocities in nitrogen.[13] Similarly, at higher pressures our measured velocities can be compared with those of nitrogen recorded up to 1 GPa (Ref. 14) and up to the liquid–solid phase boundary.[15] To the upper limits of the reduced pressure of the latter study (equivalent in oxygen to 2.4 GPa at 30 °C and 3.3 GPa at 120 °C), and within the mutual uncertainty of 1%, the velocities in oxygen and in nitrogen are equal at equivalent reduced pressures and temperatures.

The ratios of the critical pressures, temperatures and densities are, respectively, 1.484, 1.224 96, and 1.219 for oxygen to nitrogen.[16] In an attempt to better the correspondence between the two EOS we used these ratios as free parameters in a simultaneous least-squares fit of the densities and heat capacities up to 0.08 GPa (and 243–303 K) in O_2 and the speeds of sound at higher pressures. The results of the best fit, 1.4787, 1.2298, and 1.220, differ little from the critical ratios; the only significant effect is to lower from 1% to 0.3% the maximum fractional difference between the previously measured densities of the two fluids.

The high-pressure EOS of oxygen was constructed as follows. Initial densities and heat capacities were taken as those of nitrogen, scaled by the optimized parameters given in the previous paragraph. Our measured speeds of sound were then fit to smooth curves with the 30 °C data extended into the metastable region and forced to converge on the 200 °C data. Since the high-pressure data for nitrogen does not extend to the equivalent in oxygen of 200 °C, we interpolated the velocities linearly in temperature to give a set of points between 30 and 100 °C. Equations (1) were then recursively integrated until a stable solution was achieved. The starting pressure of the integration was 0.8 GPa, the lowest

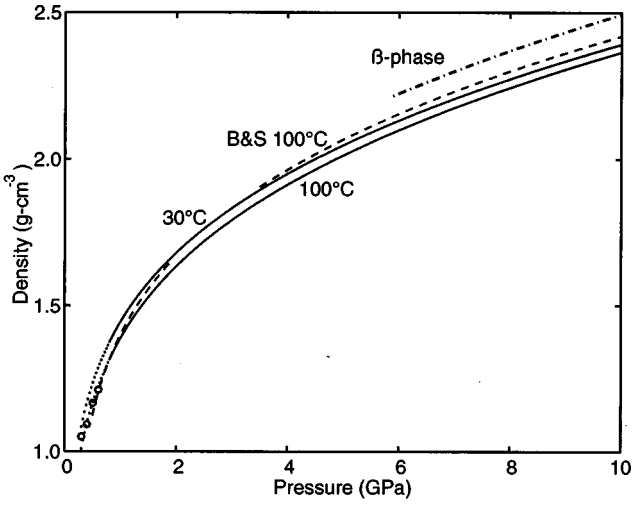

FIG. 4. Density is plotted against pressure. The results of our model are shown at 30 °C (upper solid line) and 100 °C (lower solid line). The dashed line (B&S) represents the results of Ref. 17 at 100 °C, while the dot-dashed line gives the density of the β phase (Ref. 12) at 30 °C. At the lower pressures the circles represent measured densities at 100 °C as reported in Ref. 8 and the dotted lines depict the corresponding densities of fluid nitrogen (Ref. 15), scaled as described in the text.

for which our data are complete. If, instead, we begin the integration at 2.4 GPa, the highest for which equivalent data on nitrogen exist, the calculated densities are greater by 0.4% from 2.4 GPa to 10 GPa. Calculated densities along the 30 and 100 °C isotherms are plotted in Fig. 4; beyond, respectively, 6.0 and 7.8 GPa the lines represent metastable states. These curves were fitted to the form

$$\sum_{n=0}^{3} a_n[\ln(P+P_0)]^n \tag{2}$$

with the constants given in Table II and a maximum fractional deviation of 4×10^{-5}. The densities derived from our data fall, correctly, lower than those of crystalline β-oxygen.[12]

The difficulty in inverting the velocity data into an equation of state is principally due to the large contribution of the second term in Eq. (1a), which effects the correction from an isentropic to an isothermal compressibility. While the first term is directly calculated from the velocities with an uncertainty of $<0.5\%$, the second is derived from the variation of velocity with temperature, with much larger fractional uncertainties. For a less compressible fluid the second term would contribute little to the integral, but in this pressure regime oxygen is still fairly soft and the contribution of the integrated ''correction'' is significant; at 10 GPa it is about 7% of the total calculated density. Since much of the uncertainty lies in systematic errors (such as from the extrapolation of the 30 °C velocities into the metastable region) it is difficult to make an exact estimate of it, however, based on the sensitivity of the results to small variations in the model, we give a probable error in density of 2% at 10 GPa.

TABLE II. Parameters for Eq. (2), which gives the calculated density (g cm^{-3}) as a function of pressure (GPa) between 0.8 and 10.0 GPa. The parenthetic numerals indicate a power of ten by which each number should be multiplied.

T (°C)	30	100
P_0	0.0440 (0)	0.0294 (0)
a_0	1.4294 (0)	1.3774 (0)
a_1	3.3478 (−1)	3.4845 (−1)
a_2	1.4381 (−2)	1.2202 (−2)
a_3	9.2085 (−3)	9.6840 (−3)

A PVT surface for high-pressure oxygen has also been developed by Belonoshko and Saxena[17] who used a molecular dynamics simulation, based on an exponential-6 potential constrained by the data of Ref. 8. A single isotherm from this surface, at 100 °C, is shown in Fig. 4; it differs from our results by about 3% at the highest pressures. Actually, these calculations were offered for temperatures over 127 °C (and pressures over 0.5 GPa), but the differences are clearly not due to the short extrapolation. A more direct comparison with data can be made through calculated sound velocities which are implicit in their results, given reasonable values of C_p at 0.5 GPa. Both the known EOS of oxygen[2] and that of nitrogen[13] (suitably scaled) give heat capacities of 37 J/K^{-1}/mole^{-1} when extrapolated to 200 °C. The speeds of sound then inferred from the equation of Belonoshko and Saxena are uniformly low, from ~20% at 0.5 GPa to ~2% at 11 GPa. This discrepancy does not result from an incorrect estimate of the initial C_p, as shown by trial variations of the value. The simulations underestimate the isothermal bulk modulus or the thermal expansion. The form of the intermolecular potential which gave rise to these results was the same as that used[18] to calculate the Hugoniot of shocked oxygen, but the parameters differ significantly. It would be interesting to see the extent to which this isotropic potential, which reproduced the shockwave data to within its experimental uncertainty, is capable of reproducing our results under conditions where the energetic barriers to rotation are expected to be comparable to kT.

A quasiharmonic lattice model gives all thermodynamic parameters of the β phase as functions of volume and temperature. Thus the fluid EOS can be used in conjunction with our previous lattice dynamical models[12] for β-oxygen to calculate the entropy and volume change, and hence a slope for the phase boundary; this may then be compared with experiment. The lattice models, which reproduce the long wave results exactly and the libron within experimental uncertainty, were developed using several alternate assumptions about the interactions of atoms with their near neighbors. In particular, our first model considered possible interactions only with the first three nearest neighbors while the second model dropped the noncentral terms between atoms in the same molecule in favor of the more intuitive central force between fourth nearest neighbors.

In order to determine the appropriate entropies and volumes of melting a volume was chosen in the β phase and (starting at room temperature where pressures and densities are known from the combination of x-ray[19] and velocity[12] data) thermal pressures as predicted by the models were used to extend the isochore to the melting line. The intersection of the solid isochore with the melting line gave the pressures and temperatures at which the entropy and volume of melt-

ing were evaluated. This procedure was followed for two isochores of 2.232 and 2.342 g/cm^{-3} which are plotted, for lattice model 1, in Fig. 4. Both models gave constant melting slopes, of 3.5×10^{-2} and 2.6×10^{-2} GPa/K^{-1} respectively; these may be compared with the experimental value of 2.7×10^{-2} GPa/K^{-1}. The difference between the slopes predicted by the two models is due mostly to the differences in calculated entropy of the solid, rather than the small differences between the points of intersection.

CONCLUSIONS

Velocities of sound in fluid oxygen have been measured to 200 °C and 11 GPa. In addition, the fluid-β phase boundary has been more precisely established with respect to the ruby pressure scale. These data, taken at higher pressures than previously accessible to quasistatic velocity measurements, form a basis for the development and validation of calculational techniques which may be used to predict the properties of dense fluids, particularly in a regime where angular isotropy may not be a valid approximation. Over the limited range in which data exist both for oxygen and nitrogen the principle of correspondence of states continues to hold for their velocities within experimental error. An approximate equation of state developed on the basis of these data indicates that at the higher pressures the fluid has been compressed to densities over twice that of the cryogenic liquid.

ACKNOWLEDGMENTS

This work was supported by Grant Nos. EAR 96-14313 and EAR 94-18827 from the National Science Foundation and by research subcontract B5030002 from Lawrence Livermore National Laboratory.

[1] W. Wagner, K. M. de Reuck, and S. Angus, *Oxygen: International Thermodynamic Tables of the Fluid State* (Blackwell Scientific, Oxford, 1987), Vol. 9.
[2] R. Schmidt and W. Wagner, Fluid Phase Equilibria **19**, 175–200 (1985).
[3] L. A. Weber, J. Res. Natl. Bur. Stand., Sect. A **74**, 93–129 (1970).
[4] L. A. Weber, NASA (1977).
[5] J. Ewers, dissertation (Ruhr-Universitaet, Bochum, 1981).
[6] R. D. Goodwin and L. A. Weber, J. Res. Natl. Bur. Stand., Sect. A **73**, 15–24 (1969).
[7] G. C. Straty and B. A. Younglove, J. Chem. Thermodyn. **5**, 305–12 (1973).
[8] D. S. Tsiklis and A. I. Kulikova, Russ. J. Phys. Chem. **39**, 928–30 (1965).
[9] W. J. Nellis and A. C. Mitchell, J. Chem. Phys. **73**, 6137–45 (1980).
[10] H. K. Mao, P. M. Bell, J. W. Shaner, and D. J. Steinberg, J. Appl. Phys. **49**, 3276–83 (1978).
[11] R. G. Munro, G. J. Piermarini, S. Block, and W. B. Holzapfel, J. Appl. Phys. **57**, 165–169 (1985).
[12] E. H. Abramson, L. J. Slutsky, and J. M. Brown, J. Chem. Phys. **100**, 4518–26 (1994).
[13] S. Angus, K. M. de Reuck, and B. Armstrong, *International Thermodynamic Tables of the Fluid State-6: Nitrogen* (Pergamon, Oxford, 1979).
[14] P. J. Kortbeek, N. J. Trappeniers, and S. N. Biswas, Int. J. Thermophys. **9**, 103–16 (1988).
[15] R. L. Mills, D. H. Liebenberg, and J. C. Bronson, J. Chem. Phys. **63**, 1198–204 (1975).
[16] R. T. Jacobsen, S. G. Penoncello, and E. W. Lemmon, *Thermodynamic Properties of Cryogenic Fluids* (Plenum, New York, 1997).
[17] A. Belonoshko and S. K. Saxena, Geochim. Cosmochim. Acta **55**, 3191–3208 (1991).
[18] M. Ross and F. H. Ree, J. Chem. Phys. **73**, 6146–52 (1980).
[19] D. Schiferl, D. T. Cromer, and R. L. Mills, Acta Crystallogr. **B37**, 1329–32 (1981).
[20] J. Yen and M. Nicol, J. Phys. Chem. **91**, 3336–41 (1987).